arXiv:1612.05901v1 [physics.comp-ph] 18 Dec 2016

Entropically Damped Artificial Compressibility for SPH

Prabhu Ramachandran[a,*], Kunal Puri[b]

[a]*Department of Aerospace Engineering, Indian Institute of Technology Bombay, Powai, Mumbai 400076*
[b]*Department of Mechanical Engineering, Technion, Israel Institute of Technology, Haifa, Israel 3200003*

Abstract

In this paper, the Entropically Damped Artificial Compressibility (EDAC) formulation of Clausen (2013) is used in the context of the Smoothed Particle Hydrodynamics (SPH) method for the simulation of incompressible fluids. Traditionally, weakly-compressible SPH (WCSPH) formulations have employed artificial compressiblity to simulate incompressible fluids. EDAC is an alternative to the artificial compressiblity scheme wherein a pressure evolution equation is solved in lieu of coupling the fluid density to the pressure by an equation of state. The method is explicit and is easy to incorporate into existing SPH solvers using the WCSPH formulation. This is demonstrated by coupling the EDAC scheme with the recently proposed Transport Velocity Formulation (TVF) of Adami et al. (2013). The method works for both internal flows and for flows with a free surface (a drawback of the TVF scheme). Several benchmark problems are considered to evaluate the proposed scheme and it is found that the EDAC scheme gives results that are as good or sometimes better than those produced by the TVF or standard WCSPH. The scheme is robust and produces smooth pressure distributions and does not require the use of an artificial viscosity in the momentum equation although using some artificial viscosity is beneficial.

Keywords: SPH, Entropically Damped Artificial Compressibility, Artificial Compressibility, Free Surface Flows

*Corresponding author
Email addresses: prabhu@aero.iitb.ac.in (Prabhu Ramachandran), kunal.r.puri@gmail.com (Kunal Puri)

1. Introduction

The Smoothed Particle Hydrodynamics (SPH) technique was initially developed for astrophysical problems independently by Lucy [1], and Gingold and Monaghan [2]. The method is grid-free and self-adaptive. With the introduction of the weakly-compressible SPH scheme (WCSPH) by Monaghan [3], the SPH method has been extensively applied to incompressible fluid flow and free-surface problems (see [4] and [5] for a recent review with an emphasis on the application of SPH to industrial fluid flow problems). Alternative to the WCSPH approach, pressure-based implicit SPH schemes like the projection-SPH [6] and incompressible-SPH [7] have also been introduced. These methods force the incompressiblity constraint ($\nabla \cdot \mathbf{u} = 0$) by solving a pressure-Poisson equation. While generally considered to be more accurate, the implicit nature of these schemes makes it difficult to implement and parallelize which has lead to the WCSPH approach garnering favor within the SPH community.

The weakly-compressible formulation relies on a stiff equation of state (usually referred as the Tait's equation of state in the SPH literature) that generates large pressure changes for small density variations. A consequence is that the large pressure oscillations need to be damped out, which necessitate the use of some form of artificial viscosity. Another problem with the WCSPH formulation is the appearance of void regions and particle clumping, especially where the pressure is negative. This has resulted in some researchers using problem-specific background pressure values to mitigate this problem. The Transport Velocity Formulation (TVF) of Adami et al. [8] ameliorates some of the above issues by ensuring a more homogeneous distribution of particles by introducing a background pressure field. This background pressure is not tuned to any particular problem. In addition, the particles are moved using an advection (transport) velocity instead of the actual velocity. The advection velocity differs from the momentum velocity by the constant background pressure. The motion induced by the background pressure is corrected by introducing an additional stress term in the momentum equation. The stiffness of the state equation is reduced by using a value of $\gamma = 1$ in the equation of state in contrast to the traditionally chosen value of $\gamma = 7$. The scheme produces excellent results for internal flows and virtually eliminates particle clumping and void regions. The scheme also displays reduced pressure oscillations. Unfortunately, the scheme does not work for free-surface flows and this is a significant disadvantage.

The Entropically Damped Artificially Compressible (EDAC) method of Clausen [9, 10] is an alternative to the artificial compressibility used by the weakly-compressible formulation. This method is similar to the kinetically reduced local Navier-Stokes method presented in [11, 12, 13]. However, the EDAC scheme uses the pressure instead of the grand potential as the thermodynamic variable and this simplifies the resulting equations. The EDAC scheme does not rely on an equation of state that relates pressure to density. Instead, an evolution equation for the pressure is derived based on thermodynamic considerations. This equation includes a damping term for the pressure which reduces pressure oscillations significantly. The scheme in its original form does not introduce any new parameters into the simulation. There is also no need to introduce an artificial viscosity in the momentum equation. The method has been tested in finite-difference [9] and finite-element [10] schemes and appears to produce good results.

In this work, the EDAC method is applied to SPH for the simulation of incompressible fluids for both internal and free-surface problems. The motivation for this work arose from the encouraging (despite a relatively naive implementation) results presented in [14]. In that work, we found that a simple application of the EDAC scheme produced results that were better than the standard WCSPH, though not better than those of the TVF scheme. Upon further investigation, it was found that when the background pressure used in the TVF formulation is set to zero, the EDAC scheme outperforms it. This is because the EDAC scheme provides a smoother pressure distribution than that which is obtained via the equation of state. There is still no mechanism within the EDAC framework to ensure a uniform distribution of particles however. Therefore, we adapted the TVF scheme to be used along with EDAC. The resulting scheme produces very good results and outperforms the standard TVF for many of the benchmark problems considered in this work.

The proposed EDAC scheme thus comes in two flavors. For internal flows, a formulation based on the TVF is employed where a background pressure is added. This background pressure ensures a homogeneous particle distribution. For free-surface flows, a straight-forward formulation is used with the EDAC to produce very good results. The scheme thus works well for both internal and external flows. Several results are presented along with suitable comparisons between the TVF and standard SPH schemes to demonstrate the new scheme. All the results presented in this work are reproducible through the publicly available PySPH package [15, 16] along

with the code in `http://gitlab.com/prabhu/edac_sph`.

The paper is organized as follows. In Section 2, the governing equations for the EDAC scheme are outlined. In Section 3, the SPH discretization for the EDAC equations are presented. In Section 4, the new scheme is evaluated against a suite benchmark problems of increasing complexity. The results are compared to the analytical solution where available, and to the traditional WCSPH and TVF formulations wherever possible. In Section 5, the paper is concluded with a summary and an outline for further work.

2. The EDAC method

The EDAC method is discussed in detail in [9, 10]. In this method, the density of the fluid ρ is held fixed and an evolution equation for the pressure based on thermodynamic considerations is derived. As a result, a pressure evolution equation needs to be solved in addition to the momentum equation. The equations are,

$$\frac{d\mathbf{u}}{dt} = -\frac{1}{\rho}\nabla p + \text{div}(\sigma), \tag{1}$$

$$\frac{dp}{dt} = -\rho c_s^2 \text{div}(\mathbf{u}) + \nu \nabla^2 p, \tag{2}$$

where $\mathbf{u}$ is the velocity of the fluid, p is the pressure, σ is the deviatoric part of the stress tensor, c_s is the speed of sound, and ν is the kinematic viscosity of the fluid. The material derivative is defined as,

$$\frac{d(\cdot)}{dt} = \frac{\partial(\cdot)}{\partial t} + \mathbf{u} \cdot \text{grad}(\cdot). \tag{3}$$

As is typically chosen in WCSPH schemes, the speed of sound is set to a multiple of the maximum fluid velocity. In this paper $c_s = 10\ u_{\max}$ unless otherwise mentioned.

In this work, the fluid is assumed to be Newtonian, which results in the following momentum equation:

$$\frac{d\mathbf{u}}{dt} = -\frac{1}{\rho}\nabla p + \nu \nabla^2 \mathbf{u}. \tag{4}$$

On comparison with the standard WCSPH formulation, it can be seen that the momentum equation is unchanged and equation (2) replaces the continuity equation $\frac{d\rho}{dt} = -\rho(\nabla \cdot \mathbf{u})$ in the EDAC method. Also, owing to the

pressure evolution equation in EDAC, there is no need for an equation of state to couple the fluid density and pressure.

In the next section, an SPH-discretization of these equations is performed to obtain the numerical scheme.

3. Numerical implementation

As discussed in the introduction, there are two major issues that arise when using weakly-compressible SPH (WCSPH) formulations. The first is the presence of large pressure oscillations due to the stiff equation of state and the second is due to the inhomogeneous particle distributions. The basic EDAC formulation solves the first problem [14]. The TVF scheme solves the second problem by the introduction of a background pressure for internal flows. Based on this, two different formulations using the EDAC are presented in the following. The first formulation is what we call the *standard EDAC formulation*. This formulation can be used for external flows. The second formulation is what we call the *EDAC TVF formulation*, which is based on the TVF formulation and can be applied to internal flows where it is possible to use a background pressure. Numerical discretizations for both these schemes are discussed next.

3.1. The standard EDAC formulation

The EDAC formulation keeps the density constant and this eliminates the need for the continuity equation or the use of a summation density to find the pressure. However, in SPH discretizations, m/ρ is typically used as a proxy for the particle volume. The density of the fluids can therefore be computed using the summation density approach. This density does not directly affect the pressure as there is no equation of state. In the case of solid walls, the density of any wall particle is set to a constant. The classic summation density equation for SPH is recalled:

$$\rho_i = \sum_j m_j W_{ij}, \tag{5}$$

where $W_{ij} = W(|\mathbf{r_i} - \mathbf{r_j}|, h)$ is the kernel function chosen for the SPH discretization and h is the kernel radius parameter. In this paper, the quintic

spline kernel is used, which is given by,

$$W(q) = \begin{cases} \alpha_2 \left[(3-q)^5 - 6(2-q)^5 + 15(1-q)^5\right], & \text{for } 0 \le q \le 1, \\ \alpha_2 \left[(3-q)^5 - 6(2-q)^5\right], & \text{for } 1 < q \le 2, \\ \alpha_2 \, (3-q)^5, & \text{for } 2 < q \le 3, \\ 0, & \text{for } q > 3, \end{cases} \tag{6}$$

where $\alpha_2 = 7/(478\pi h^2)$ in 2D.

In the previous work [14], Monaghan's original formulation was used for the pressure gradient and the formulation due to Morris et al. [17] was used for the viscous term in equation (4). The method of Adami et al. [18] was used to implement the effect of boundaries.

In the present work, a number density based formulation is employed as used in [18], which results in the following momentum equation:

$$\frac{d\mathbf{u}_i}{dt} = \frac{1}{m_i} \sum_j \left(V_i^2 + V_j^2\right) \left[-\tilde{p}_{ij} \nabla W_{ij} + \tilde{\eta}_{ij} \frac{\mathbf{u}_{ij}}{(r_{ij}^2 + \eta h_{ij}^2)} \nabla W_{ij} \cdot \mathbf{r}_{ij}\right] + \mathbf{g}_i, \tag{7}$$

where $\mathbf{r}_{ij} = \mathbf{r}_i - \mathbf{r}_j$, $\mathbf{u}_{ij} = \mathbf{u}_i - \mathbf{u}_j$, $h_{ij} = (h_i + h_j)/2$, $\eta = 0.01$,

$$V_i = \frac{1}{\sum_j W_{ij}}, \tag{8}$$

$$\tilde{p}_{ij} = \frac{\rho_j p_i + \rho_i p_j}{\rho_i + \rho_j}, \tag{9}$$

$$\tilde{\eta}_{ij} = \frac{2\eta_i \eta_j}{\eta_i + \eta_j}, \tag{10}$$

where $\eta_i = \rho_i \nu_i$.

The EDAC pressure evolution equation (2) is discretized using a similar approach to the momentum equation to be,

$$\frac{dp_i}{dt} = \sum_j \frac{m_j \rho_i}{\rho_j} c_s^2 \, \mathbf{u_{ij}} \cdot \nabla W_{ij} + \frac{(V_i^2 + V_j^2)}{m_i} \tilde{\eta}_{ij} \frac{p_{ij}}{(r_{ij}^2 + \eta h_{ij}^2)} \nabla W_{ij} \cdot \mathbf{r}_{ij}, \tag{11}$$

where $p_{ij} = p_i - p_j$. The particles are moved according to,

$$\frac{d\mathbf{r}_i}{dt} = \mathbf{u}_i. \tag{12}$$

Upon the specification of suitable initial conditions for $\mathbf{u}$, p, m, and $\mathbf{r}$, equations (5), (7), (11), and (12) are sufficient for simulating the flow in the absence of any boundaries.

3.2. EDAC TVF formulation

In WCSPH, as the particles move they tend to become disordered. This introduces significant errors in the simulation. The particle positions can be regularized by the addition of a background pressure. A naive approach would be to simply add a constant pressure and use it in the governing equations. However, this does not work well in practice as the SPH pressure derivative is not accurate when the pressures are large [19]. The TVF scheme of Adami et al. [8] overcomes this by advecting the particles using an arbitrary background pressure through the "transport velocity" and correct for this background pressure using an additional stress term in the momentum equation. This ensures a homogeneous particle distribution without introducing a constant background pressure in the pressure derivative term.

For internal flows, the TVF formulation is adapted to introduce the background pressure. The density is computed using the summation density equation (5). As before, this is mainly to serve as a proxy for the particle volume in the SPH discretizations. The momentum equation for the TVF scheme as discussed in Adami et al. [8] is given by,

$$\frac{\tilde{d}\mathbf{u}_i}{dt} = \frac{1}{m_i}\sum_j \left(V_i^2 + V_j^2\right)\Bigg[-\tilde{p}_{ij}\nabla W_{ij} + \frac{1}{2}(\mathbf{A}_i + \mathbf{A}_j)\cdot\nabla W_{ij} + \tilde{\eta}_{ij}\frac{\mathbf{u}_{ij}}{(r_{ij}^2 + \eta h_{ij}^2)}\nabla W_{ij}\cdot\mathbf{r}_{ij}\Bigg] + \mathbf{g}_i, \tag{13}$$

where $\mathbf{A} = \rho\mathbf{u}(\tilde{\mathbf{u}} - \mathbf{u})$, $\tilde{\mathbf{u}}$ is the advection or transport velocity and the material derivative, $\frac{\tilde{d}}{dt}$ is given as,

$$\frac{\tilde{d}(\cdot)}{dt} = \frac{\partial(\cdot)}{\partial t} + \tilde{\mathbf{u}}\cdot\text{grad}(\cdot). \tag{14}$$

Thus the particles move using the transport velocity,

$$\frac{d\mathbf{r}_i}{dt} = \tilde{\mathbf{u}}_i. \tag{15}$$

The transport velocity is obtained from the momentum velocity $\mathbf{u}$ at each time step using,

$$\tilde{\mathbf{u}}_i(t+\delta t) = \mathbf{u}_i(t) + \delta t\left(\frac{\tilde{d}\mathbf{u}_i}{dt} - \frac{p_b}{m_i}\sum_j \left(V_i^2 + V_j^2\right)\nabla W_{ij}\right), \tag{16}$$

where p_b is the background pressure.

In the TVF scheme, the pressure is computed from the density using the standard equation of state with a value of $\gamma = 1$. Instead, the EDAC equation (11) is used to evolve the pressure. In the present approach, the pressure reduction technique proposed by Basa et al. [19] is used to mitigate the errors due to large pressures. This requires the computation of the average pressure of each particle, p_{avg}:

$$p_{\text{avg},i} = \sum_{j=1}^{N_i} \frac{p_j}{N_i}, \tag{17}$$

where N_i are the number of neighbors for the particle i and includes both fluid and boundary neighbors. Equation (9) is then replaced with,

$$\tilde{p}_{ij} = \frac{\rho_j(p_i - p_{avg,i}) + \rho_i(p_j - p_{avg,i})}{\rho_i + \rho_j}. \tag{18}$$

In Section 4 it can be seen that this results in significantly improved results that outperform the traditional TVF scheme. It is worth mentioning that this technique, applied to the standard SPH or to the standard TVF scheme does not result in any significant improvement.

The boundary conditions are satisfied using the formulation of Adami et al. [18]. This method uses fixed wall particles and sets the pressure and velocity of these wall particles in order to accurately simulate the boundary conditions. The same scheme is used here with the only modification being that the density of the boundary particles is not set based on the pressure of the boundary particles (i.e. equation (28) in Adami et al. [18] is not used).

3.3. Suitable choice of ν for EDAC

In equation (11) one can see that the viscosity ν is used to diffuse the pressure. The original formulation assumes that the value of ν is the same as the fluid viscosity. In practice it is found that if the viscosity is too small, the pressure builds up too fast and eventually blows up. If the viscosity is too large it diffuses too fast resulting in a non-physical simulation. Thus, the physical viscosity is not always the most appropriate. Instead using,

$$\nu_{edac} = \frac{\alpha h c_s}{8}, \tag{19}$$

works very well. The choice of ν_{edac} is motivated by the expression for artificial viscosity in traditional WCSPH formulations. In this paper, it is found

that $\alpha = 0.5$ is a good choice for a wide range of Reynolds numbers (0.0125 to 10000).

To summarize the schemes,

- for external flow problems, equations (5), (7), and (11) are used. The particles move with the fluid velocity $\mathbf{u}$ and are advected according to (12).

- for internal flows, equations (5), (13), (17), (18) and (11) are used. Equation (15) is used to advect the particles. The transport velocity is found from equation (16).

For each of the schemes, the value of ν used in the equation (11) is found using equation (19). The value of ν used in the momentum equation is the fluid viscosity.

The proposed EDAC scheme is explicit and as such, any suitable integrator can be used. In this work, one of the two simplest possible two-stage explicit integrators is chosen. For both integrators, the particle properties are first predicted at $t + \delta t/2$. The right-hand-side (RHS) is subsequently evaluated at this intermediate step and the final properties at $t + \delta t$ are obtained by correcting the predicted values. We define two variants of this predictor-corrector integration scheme. In the first type, the prediction stage is completed using the RHS from the previous time-step. We call it the Predict-Evaluate-Correct (PEC) type integrator. In the second variant, an evaluation of the RHS is carried out for the predictor stage. This integrator, deemed Evaluate-Predict-Evaluate-Correct (EPEC) is more accurate (at the cost of two RHS evaluations per time-step).

As mentioned in the introduction, all the equations and algorithms presented in this work are implemented using the PySPH framework [15, 16, 20]. PySPH is an open source framework for SPH that is written in Python. It is easy to use, easy to extend, and supports non-intrusive parallelization and dynamic load balancing. PySPH provides an implementation of the TVF formulation and this allows for a comparison of the results with those of the standard SPH and TVF where necessary. In the next section, the performance of the proposed SPH scheme is evaluated for several benchmark problems of varying complexity.

4. Numerical Results

In this section the EDAC scheme is applied to a suite of test problems. The results from the new EDAC scheme are compared with the standard weakly compressible SPH (WCSPH) and, where possible, with those from the Transport-Velocity-Formulation (TVF) scheme [8].

Every attempt has been made to allow easy reproduction of all of the present results. The TVF implementation is available as part of PySPH [20]. The implementation of EDAC-SPH will eventually be merged into PySPH. Every figure in this article is automatically generated. The approach and tools used for this are described in detail in a forthcoming article. The code for the EDAC implementation and the automation of all of our results are available from `http://gitlab.com/prabhu/edac_sph`.

4.1. Couette and Poiseuille flow

The Couette and Poiseuille flow problems are extremely simple. They do not involve a significant motion of the particles, however, they admit an exact solution which makes it a good first benchmark problem to evaluate the proposed scheme. These problems have been used before [8] to evaluate the TVF scheme and we compare our results with theirs. The domain for these test cases is rectangular with periodic boundary conditions in the x direction. Standard no-slip wall boundary conditions [18] are imposed along the walls.

The quintic spline kernel (equation (6)) is used and the smoothing length, h, is chosen to be equal to the particle spacing, $h = \Delta x = \Delta y$. The Predict-Evaluate-Correct (PEC) integrator with a fixed time-step is used and chosen as per the following equation,

$$\Delta t = \min\left(\frac{h}{4(c + |U_{max}|)},\ \frac{h^2}{8\nu}\right). \tag{20}$$

Unless explicitly mentioned, all simulations use this integrator and a time-step chosen as above.

For the Couette flow problem, the Reynolds number is set to $Re = 0.0125$, the kinematic viscosity is chosen to be $0.01 m^2/s$ and the density is set to $1.0 kg/m^3$. The top wall is assumed to be moving with a fixed velocity of $u = Re \times \nu$. In Fig. 1 the axial velocity profile along the channel in the transverse direction is plotted at $t = 100$ seconds.

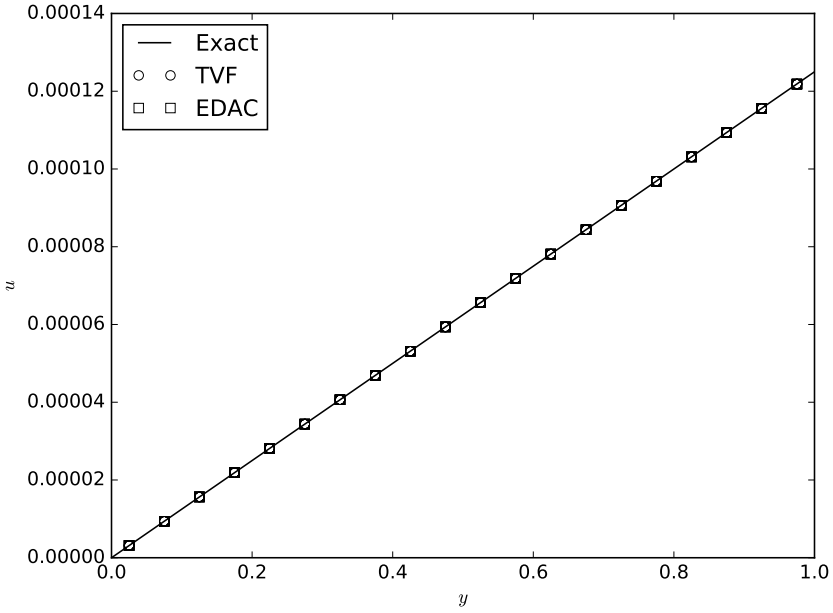

Figure 1: Axial velocity profile along the channel in the transverse (y) direction for the Couette flow problem at time $t = 100$s. A uniform distribution of particles is used with $\Delta x = 0.05$.

For the Poiseuille flow problem, the Reynolds number is again set at $Re = 0.0125$ and the kinematic viscosity is $\nu = 0.01m^2/s$. $\Delta x = 1/60$ and the smoothing length is set equal to the initial particle spacing. The quintic spline kernel is used. Fig. 2 shows the axial component of the velocity in the transverse direction along the channel at $t = 100$s. The results show that the EDAC performs as well as the TVF for these problems. It should be noted that these problems do not involve any significant motion of the particles, the results are not indicative of the efficacy of the schemes. Nevertheless, these tests show that the discretization of the EDAC-SPH equations in Section 2 is consistent with the governing equations.

4.2. Taylor Green Vortex

The Taylor-Green vortex problem is a particularly challenging case to simulate using SPH. This is an exact solution of the Navier-Stokes equations in a periodic domain. Here, a two-dimensional version is considered as is

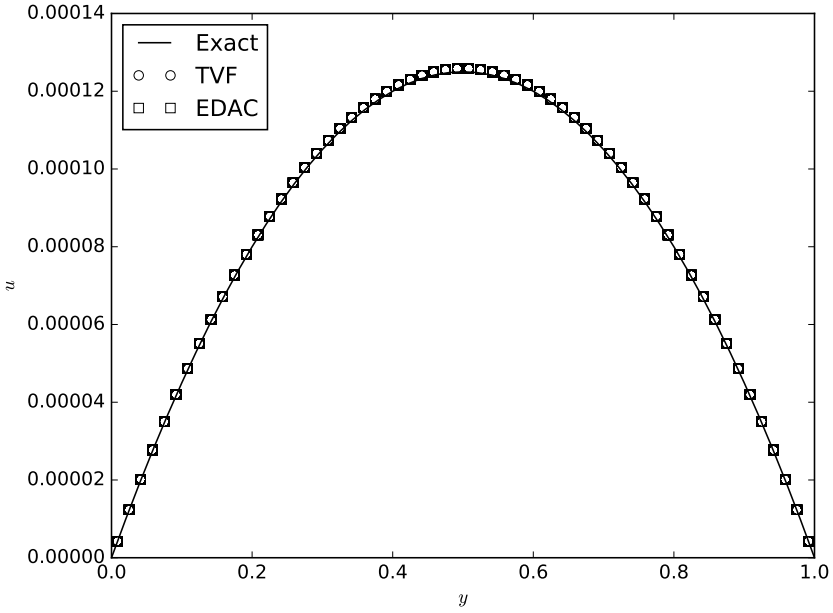

Figure 2: Axial velocity profile along the channel in the transverse direction for the Poiseuille flow problem at time $t = 100$s. A uniform distribution of particles is used with $\Delta x = 1/60$.

done in [8]. The fluid is considered periodic in both directions and the exact solution is given by,

$$u = -Ue^{bt}\cos(2\pi x)\sin(2\pi y) \tag{21}$$

$$v = Ue^{bt}\sin(2\pi x)\cos(2\pi y) \tag{22}$$

$$p = -U^2e^{2bt}(\cos(4\pi x) + \cos(4\pi y))/4, \tag{23}$$

where U is chosen as $1m/s$, $b = -8\pi^2/Re$, $Re = UL/\nu$, and $L = 1m$.

The Reynolds number, Re, is initially chosen to be 100. The flow is initialized with u, v, p set to the values at $t = 0$. The evolution of the quantities are studied for different numerical schemes. The speed of sound is set to 10 times the maximum flow velocity at $t = 0$. The background pressure is set as discussed by Adami et al. [8] to $p_b = c_s^2\rho$. The quintic spline kernel is used with the smoothing length h set to the particle spacing Δx. The value of α in the equation (19) is chosen as 0.5. The results from the standard SPH

scheme, the TVF, and the new scheme are compared. Since a physical viscosity is used and the solution to the problem remains smooth, no artificial viscosity is used for any of the schemes.

In Adami et al. [8], the simulation starts with either uniformly distributed particles or with a "relaxed initial condition". For the relaxed initial condition, the authors use the particle distribution generated by the uniformly distributed case at the final time and impose an analytical initial condition at the particle positions. The results for the uniformly distributed particles have about an order of magnitude more error than that of the relaxed initialization. This is because the uniform distribution results in particles being placed along (or near) stagnation streamlines resulting in non-uniform particle distributions.

In this work, for this particular problem, the initial distribution is uniform but a small random displacement is added to the particles. The random displacement is uniformly distributed and the maximum displacement in any coordinate direction is chosen to be $\Delta x/5$. The same initial conditions are used for all schemes. This is simple to implement, resolves the problems with stagnation streamlines, and enables for a fair comparison of all the schemes.

In Fig. 3, the decay of the maximum velocity magnitude produced by different schemes is compared with the exact solution. A regular particle distribution with $n_x = n_y = 50$ is randomly perturbed as discussed above. The standard SPH, TVF, standard EDAC (labeled EDAC ext), and TVF EDAC (labeled EDAC) schemes are compared. As can be seen, the EDAC and TVF perform best. The standard EDAC without the TVF (labeled EDAC ext) is better than the standard SPH but not as effective as the TVF scheme. As discussed in previous sections, this occurs because the TVF background pressure results in a more homogeneous particle distribution.

Fig. 3 does not clearly differentiate between schemes. The L_1 error of $|\mathbf{u}|$ is a better measure of the performance of the schemes and is plotted in Fig. 4. The L_1 error is computed as the average value of the difference between the exact velocity magnitude and the computed velocity magnitude, that is,

$$L_1 = \frac{\sum_i |\mathbf{u_{i,computed}}| - |\mathbf{u_{i,exact}}|}{\sum_i |\mathbf{u_{i,exact}}|}, \tag{24}$$

where the value of $\mathbf{u}$ is computed at the particle positions for each particle i in the flow.

Fig. 4 clearly brings out the differences in the schemes. It is easy to see that the TVF EDAC scheme (labeled EDAC) produces much lower errors

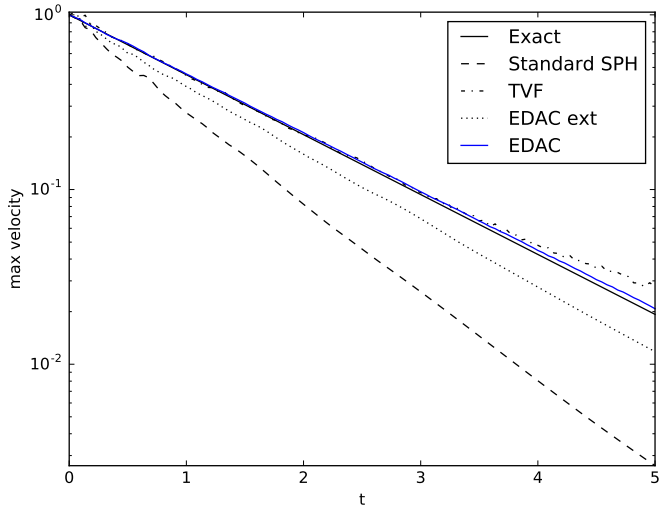

Figure 3: The decay with time of the velocity magnitude for the different schemes. Particles are initialized with $n_x = n_y = 50$ and thereafter randomly perturbed. The Reynold's number is chosen to be $Re = 100$. The quintic spline kernel is used with a smoothing length equal to the initial (undisturbed) particle spacing.

than the TVF scheme (by almost a factor of 4). The difference between the standard EDAC scheme and the TVF is also brought out. It is easy to see that the standard EDAC scheme (labeled EDAC ext) is better than the standard SPH.

In order to better understand the behavior of the methods, several other variations of the basic schemes have been studied. Fig. 5 shows the L_1 error of the velocity magnitude using the TVF formulation, along with the background pressure correction scheme of Basa et al. [19] (labeled as "TVF + BQL"). The results of using the TVF without any background pressure is labeled as "TVF (pb=0)". This clearly shows that the pressure correction of Basa et al. does not affect the TVF scheme, and that without the background pressure, the standard EDAC is in fact better than the TVF. While this is only to be expected, it does highlight that the EDAC scheme performs very well. The plot labeled "EDAC no-BQL" demonstrates that the correction due to Basa et al. is necessary for the EDAC scheme. It is also found (not shown here) that using the Basa et al. correction with the standard SPH formulation does not produce any significant advantages. Similarly, the tensile correction

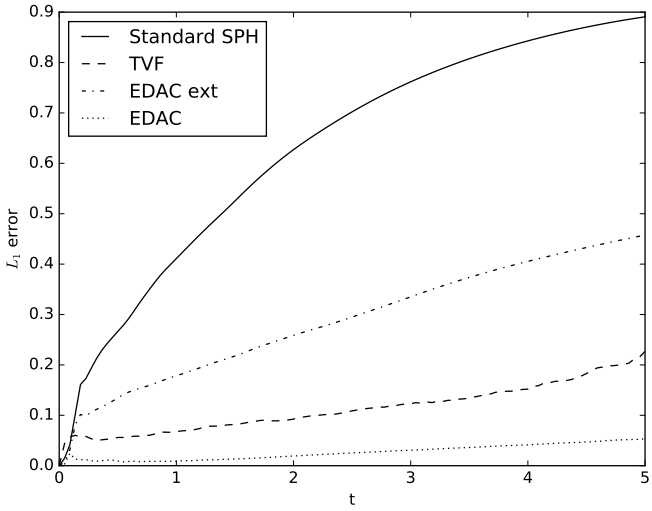

Figure 4: The L_1 error of the velocity magnitude vs. t for the standard SPH (solid line), EDAC-ext (dash-dot), EDAC (dot) and TVF (dash) schemes.

of Monaghan [21] has no major influence on the results.

The EDAC scheme evolves the pressure in a very different manner from the traditional WCSPH schemes. It is important to see how it captures the pressure field as compared with the other schemes. In Fig. 6, the L_1 error in the pressure is plotted as the simulation evolves. The pressure in the EDAC scheme drifts due to the use of the transport velocity used to move the particles, we therefore compute $p - p_{avg}$ where p_{avg} is computed using equation (17). In order to make the comparisons uniform this is done for all the schemes. This does not change the quality of the results by much. The error is computed as,

$$p_{L_1} = \frac{\sum_i |p_{i,computed} - p_{i,avg} - p_{i,exact}|}{\max_i(p_{i,exact})}. \tag{25}$$

As can be clearly seen in Fig. 6, the new EDAC scheme outperforms all other schemes. In Fig. 7, the L_1 error for the velocity magnitude is plotted but for different values of the initial particle spacing n_x. We note that $n_x = 25$ corresponds to a $\Delta x = 0.04$. As can be seen, the EDAC scheme (Section 3.2) consistently produces less error than the TVF scheme at even such low resolutions. Fig. 8 shows the distribution of particles for the case where $n_x = 100$

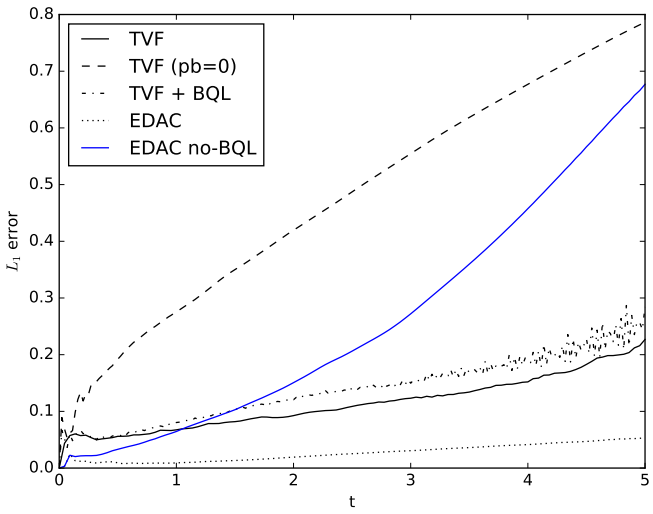

Figure 5: The L_1 error of the velocity magnitude versus t for other variations of the schemes.

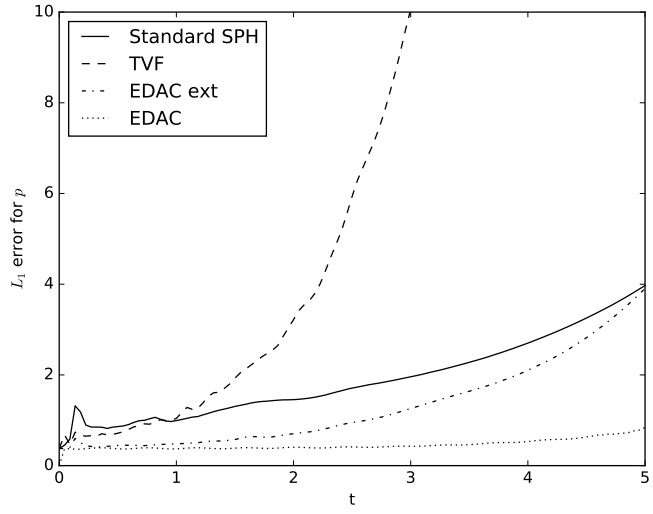

Figure 6: The L_1 error of the pressure versus t for the Standard SPH (solid line), TVF (dash), EDAC-ext (dash-dot) and EDAC (dot) schemes.

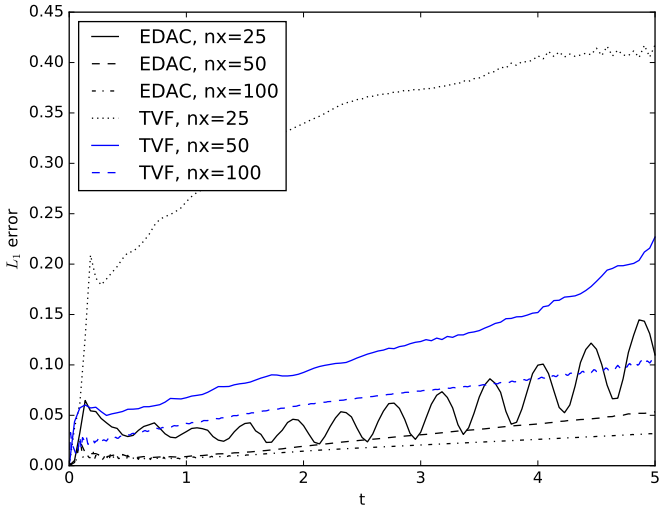

Figure 7: The L_1 error of the velocity magnitude versus t for different resolutions.

using the EDAC scheme. The color indicates the velocity magnitude. As can be seen, the particles are distributed homogeneously.

From the convergence plot it can be seen that with just 25×25 particles, the EDAC produces about 3 times less error than the TVF. It is to be noted that for this low resolution, the random initial perturbation of the particles is limited to a maximum of $\Delta x/10$ instead of the $\Delta x/5$ for the other cases.

In order to study the sensitivity of the simulations to variations in the parameter α (equation 19) used for the diffusion of the pressure in the EDAC scheme, a few simulations with $n_x = 25, Re = 100$ for different values of α are performed. If $\alpha = 0$, the fluid viscosity is used for the diffusion of pressure. The results are shown in Fig. 9. The results show that despite a variation of α by a factor of 40, the error changes by at most 60%. This suggests that a value of $\alpha = 0.5$ is a reasonable value.

Fig. 10 shows a convergence study for this problem with $Re = 1000$ and $\alpha = 1.0$. The particle spacing is increased from $n_x = 25$ to $n_x = 201$. Convergence in the L_1 norm for the velocity magnitude is visible and is verified in Fig. 11. The scheme appears to have close to second order convergence for this problem.

It is useful to compare the performance of the proposed scheme at high Reynolds numbers. To this end, simulations are performed at $Re = 10000$. A

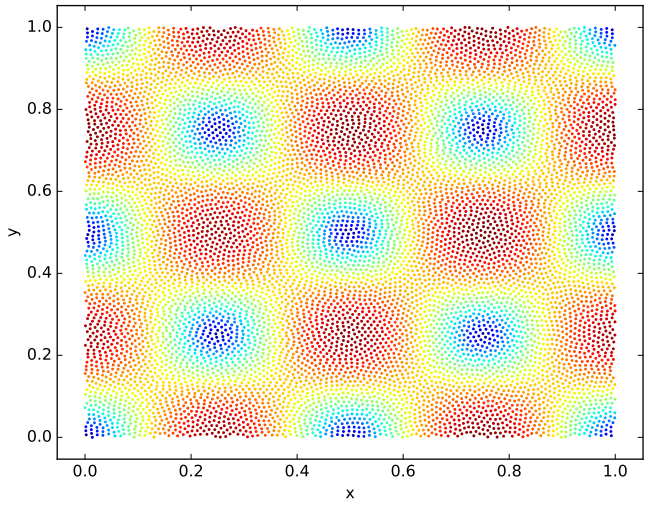

Figure 8: The distribution of particles at $t = 5$ for the simulation using the EDAC scheme with $n_x = 100$. The colors indicate the velocity magnitude.

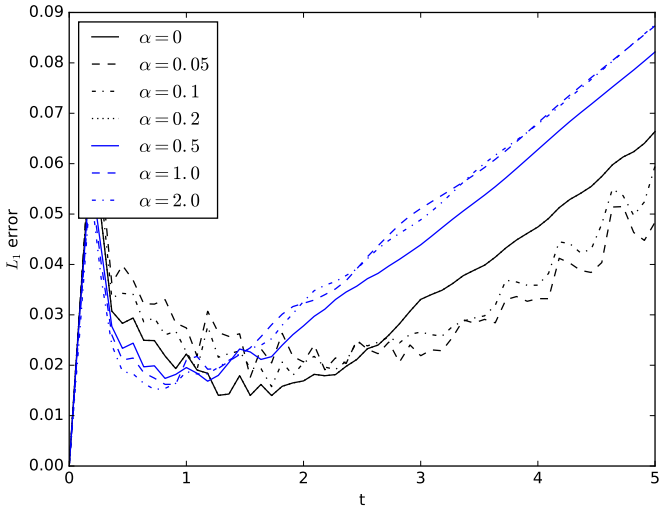

Figure 9: The L_1 error of the velocity magnitude versus t for different choices of α with $Re = 100, n_x = 25$ while using the EDAC scheme.

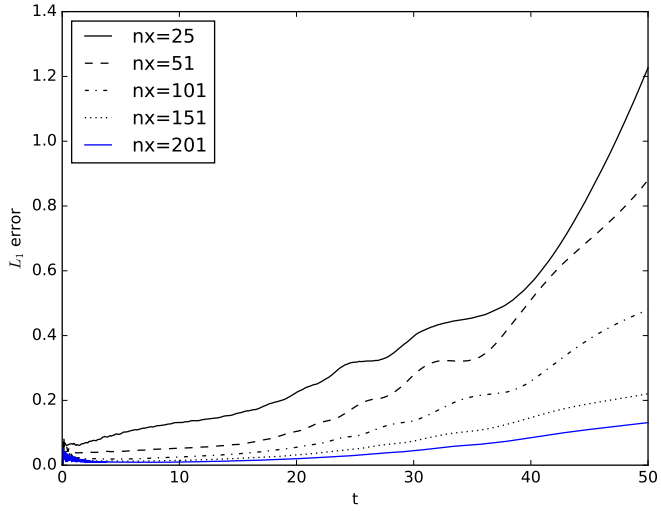

Figure 10: The L_1 error of the velocity magnitude versus t for different choices of n_x at $Re = 1000$ while using the EDAC scheme.

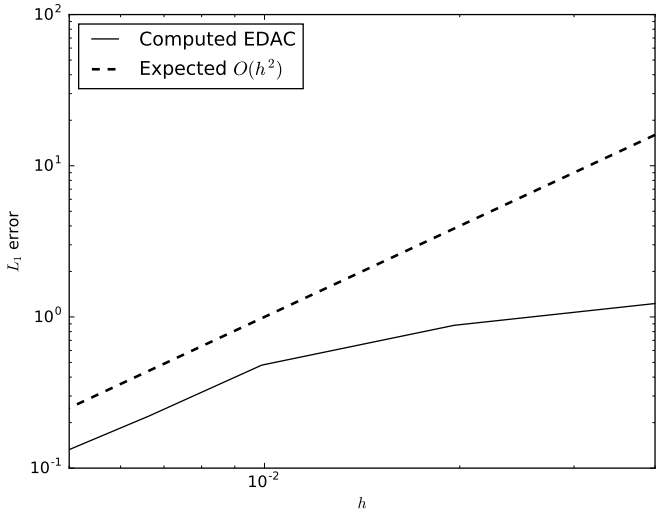

Figure 11: The L_1 error of the velocity magnitude at $t = 50$ versus h at $Re = 1000$ for the EDAC scheme. The dashed line shows the convergence of an ideal scheme with second order convergence.

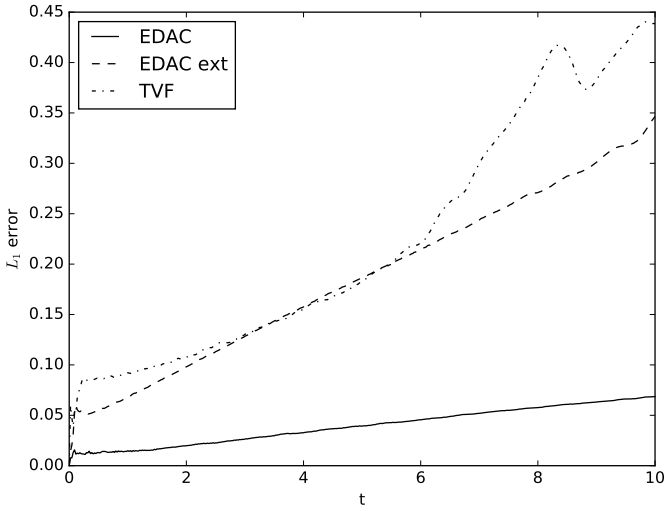

Figure 12: The L_1 error of the velocity magnitude versus t at $Re = 10000$ for the different schemes, TVF, EDAC, and EDAC external.

100x100 grid of particles is used and with a small random initial perturbation to the particles (the maximum perturbation of $\Delta x/5$ is chosen). The TVF, EDAC external and EDAC TVF schemes are compared. As can be seen in Fig. 12, the new EDAC schemes perform very well. The EDAC TVF scheme (labeled as EDAC) significantly outperforms the TVF scheme. The standard EDAC scheme (Section 3.1) performs slightly better than the TVF.

In Fig. 13 the Reynolds number is set to 10000 with $n_x = 101$. α is varied, as before, when $\alpha = 0$, the physical viscosity is used. Clearly, much better results are produced when the suggested numerical viscosity value is used instead of the physical viscosity. When the suggested value is used the results are not too sensitive to changes in α around the value of 1.

The results show that the new scheme works well and outperforms the TVF. They justify the use of the numerical viscosity, equation (19), instead of the physical viscosity while diffusing the pressure. It is also important to note that unlike the TVF, the EDAC scheme works just as well when no initial random perturbation is given to the particles.

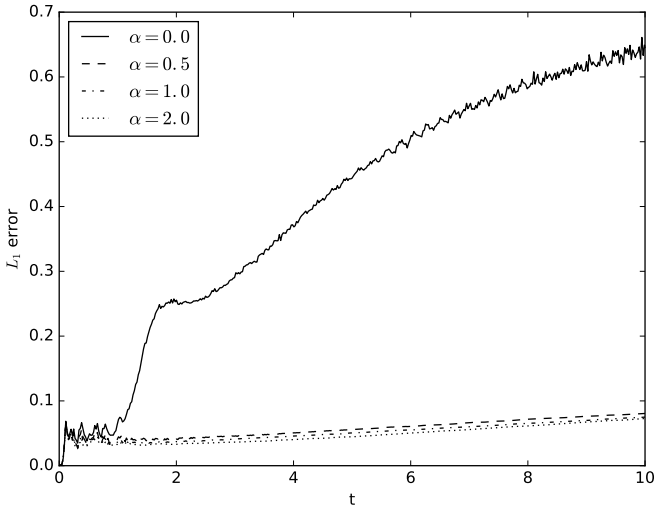

Figure 13: The L_1 error of the velocity magnitude versus t for different choices of α at $Re = 10000$ while using the EDAC scheme. When $\alpha = 0$ is used the ν_{edac} is set to the fluid viscosity ν.

4.3. Lid-Driven-Cavity

The next test problem considered is the classical Lid-Driven-Cavity (LDC) problem, which is a fairly challenging problem to simulate with SPH. The setup is simple, a unit square box with no-slip walls on the bottom, left and right boundaries. The top wall is assumed to be moving with a uniform velocity, V_{lid}, which sets the Reynolds number for the problem ($Re = \frac{V_{\text{lid}}}{\nu}$). The present scheme is studied for three different Reynold's numbers ($Re = 100, 1000, \text{and } 5000$) and the results are compared the to those of Ghia et al. [22].

For the SPH simulations, the quintic spline kernel is used with $h = \Delta x$. The PEC type predictor-corrector integrator is used with a fixed time-step, chosen according to equation (20). In addition, $\alpha = 0.5$ for all the SPH simulations. Since this problem does not involve free-surfaces, the TVF-EDAC scheme can be used (Section 3.2).

The discretization in terms of the number of particles is dependent on the Reynold's number. A uniform distribution of particles ($\Delta x = \Delta y$) is used, with a resolutions of 50×50, 100×100 and 150×150 for the $Re = 100$, $Re = 1000$ and $Re = 5000$ cases respectively. The timesteps are chosen

according to equation (20) as before.

For each case, the code is run for a sufficiently long time to reach a steady state. For the $Re = 100$ and $Re = 1000$ cases the velocity plots are made by averaging over the last 5 saved time-step results. The data is saved every 500 time-steps. The $Re = 5000$ case requires a longer run-time to reach a steady state. In this work, the final time for this case is set to $t = 250$ non-dimensional time units. The velocity plots for this case averaged over the last 250 saved time-steps (this amounts to averaging the velocity for approximately the last 19 seconds).

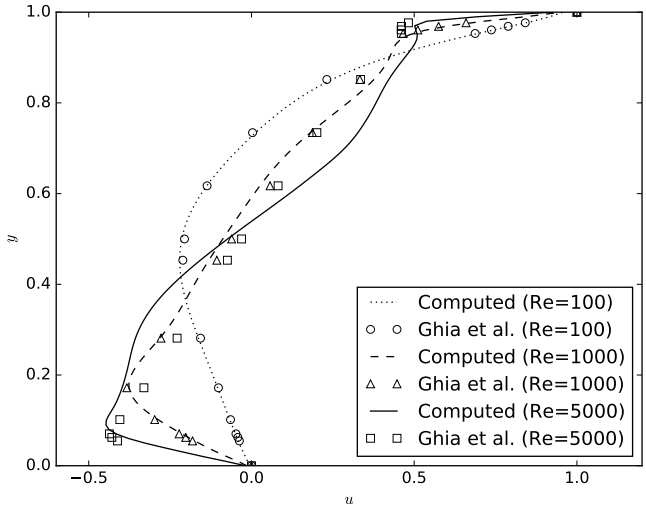

Figure 14: The velocity profile u vs. y for the lid-driven-cavity problem at different Reynolds numbers. The results are compared with those of Ghia et al. [22].

In Fig. 14, the u velocity profile along the transverse direction (y) is plotted for different Reynolds numbers along with the results of Ghia et. al Ghia et al. [22]. Similarly, in Fig. 15, the v velocity profile along the horizontal (x) direction is plotted for different Reynolds numbers. The agreement is very good for lower Reynolds numbers. For the $Re = 5000$ case the agreement is not the best. This is probably the only case in the present work for which the results with the EDAC are not better than the TVF. These simulations take a long while to run hence additional higher-resolution cases have not been simulated as the results demonstrate that the new scheme works reasonably well for this problem. We hope to explore this issue at higher Reynolds

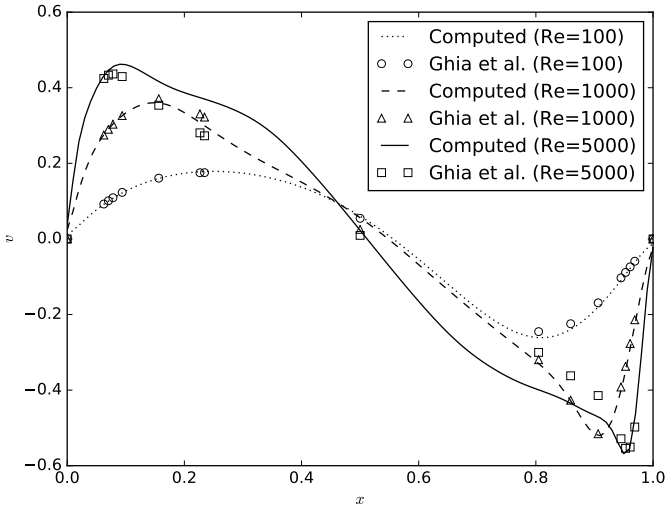

Figure 15: The velocity profile v vs. x for the lid-driven-cavity problem at different Reynolds numbers. The results are compared with those of Ghia et al. [22].

numbers in greater detail in the future.

It should be noted that at such high Reynolds numbers the use of the physical viscosity for the pressure diffusion instead of the suggested numerical viscosity will cause the particles blow up due to a lack of pressure dissipation.

4.4. Periodic lattice of cylinders

Our next case is a benchmark periodic problem in a square domain with a cylinder. The periodicity means the fluid effectively sees a periodic lattice of cylinders. This test was used to evaluate the TVF scheme in [8] and identical parameters are used for the numerical set-up. The length of the square domain is $L = 0.1m$ and the Reynold's number is set to one. A body force, $g_x = 1.5 \times 10^{-7} m/s^2$ drives the flow along the x direction. The cylinder is placed in the center of the domain with a radius $R = 0.02m$. A uniform discretization is used with 100×100 particles and a quintic spline kernel with $h = \Delta x$ is used. The PEC type predictor-corrector integrator is used with a fixed time-step chosen using equation (20).

Fig. 16 shows the axial velocity profile (u) along the lines $x = L/2$ and $x = L$, when using the TVF-EDAC scheme and compare the results with the TVF scheme. It is found that the results of the new scheme are in good

agreement with that of the TVF scheme.

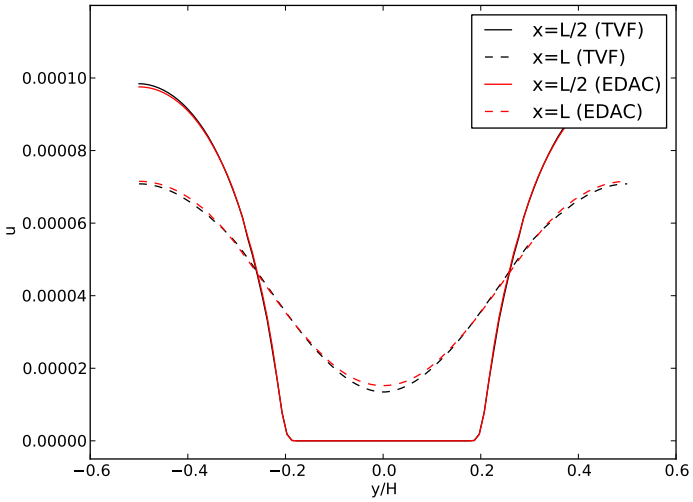

Figure 16: Axial velocity profile (u) along the transverse (y) direction at $x = L/2$ and $x = L$ for the periodic lattice of cylinders using the EDAC (red) and TVF (black) schemes.

4.5. Periodic array of cylinders

The next benchmark is similar to the periodic lattice of cylinders but with wall boundary conditions along the top and bottom walls. The domain is periodic in the x direction, driven by a body force $g_x = 2.5 \times 10^{-4} m/s^2$. A rigid cylinder with radius $R = 0.2m$ is placed in the center of the channel. The length of the channel is $L = 0.12m$ and the height is $H = 4R$. The numerical set-up is identical to that of Adami et al. [8] with $n_x = 144$ but with $h = 1.2\Delta x$ chosen for both schemes. Fig. 17 shows the drag coefficient on the cylinder generated by the TVF and the new scheme. Fig. 18 shows the distribution of the particles at the final time produced by the EDAC scheme. The particles are homogeneously distributed as would be expected. The particle distribution is very similar to that produced by Adami et al. [8].

Note that for this problem, using $c = 0.1\sqrt{g_x R}$, as recommended by Adami et al. [8] the particle positions diverge even when using the TVF formulation. Instead, in order to reproduce the results of Adami et al. [8] the value is set to $c = 0.02$m/s as recommended by Ellero and Adams [23].

The present results suggest that the EDAC scheme performs well for all of the internal flow cases. A few standard free-surface problems are considered next.

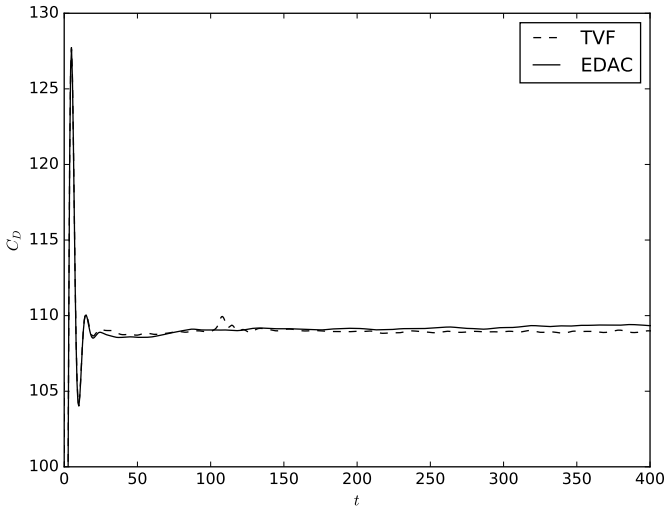

Figure 17: The drag variation C_D versus time for a periodic array of cylinders in a channel. The results from the TVF (dash) are compared with those produced by the EDAC (solid) scheme.

4.6. Elliptical drop

The elliptical drop problem is a classic problem that was first solved in the context of SPH by Monaghan [3]. The problem studies the evolution of a circular drop of inviscid fluid having unit radius in free space with the initial velocity field given by $-100x\hat{i}+100y\hat{j}$. The incompressibility constraint on the fluid enables a derivation for evolution of the semi-major axis of the ellipse. The problem is simulated with the classic WCSPH where an artificial viscosity with $\alpha = 0.1$ is used. The particle spacing is chosen to be $\Delta x = 0.025m$. A Gaussian kernel is used for the WCSPH with $h = 1.3\Delta x$. The value of $\gamma = 7$. The speed of sound is set to $1400m/s$ and $\rho = 1.0kg/m^3$. For the EDAC case, a quintic spline kernel is used with $h = 1.2\Delta x$. $\alpha = 0.5$ for the calculation of ν_{edac}. An Evaluate-Predict-Evaluate-Correct (EPEC) integration scheme is used for the WCSPH scheme whereas a Predict-Evaluate-Correct (PEC) integrator is used for the new scheme and the results are compared.

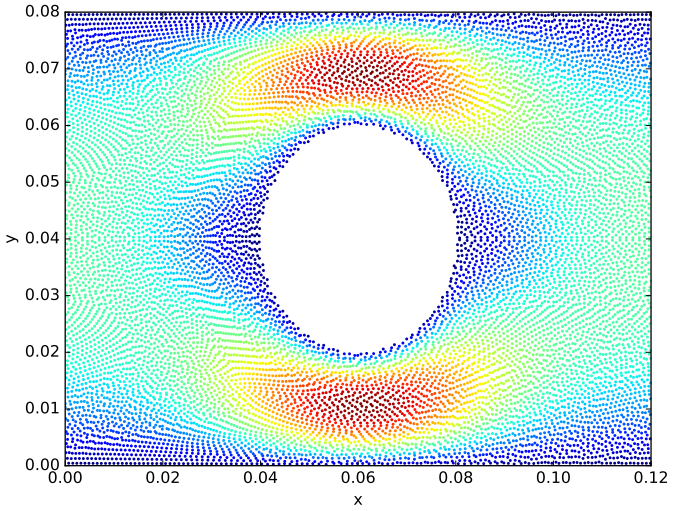

Figure 18: The distribution of particles at the final time produced by the EDAC scheme. The color indicates the velocity magnitude.

In Fig. 19, the semi-major axis of the ellipse is compared with the exact solution. The standard EDAC scheme (Section 3.1) is used to simulate the problem. $\alpha = 0.5$ and no artificial viscosity is used for the EDAC scheme. Artificial viscosity is used for the WCSPH implementation with a value of $\alpha = 0.1, \beta = 0.0$. One EDAC simulation is performed using the XSPH correction [24] and one without it. The absolute error in the size of the semi-major axis with time is used as a metric to compare the results. As can be seen, the EDAC scheme performs better than the standard SPH both with and without the XSPH correction.

In Fig. 20, the kinetic energy of the fluid is computed and plotted versus time. It is to be noted that one may obtain the exact kinetic energy by integrating the initial velocity field. Given a unit density and an initial radius of unity, this amounts to approximately 7853.98 units. The kinetic energy of the standard SPH formulation reduces due to the artificial viscosity. The EDAC scheme on the other hand does not display any significant loss of kinetic energy and the value is close to the exact value.

Fig. 21 plots the particle distribution as obtained by the WCSPH simulation. The colors show the pressure distribution. The solid line is the exact solution. Fig. 22 shows the same obtained with the EDAC without

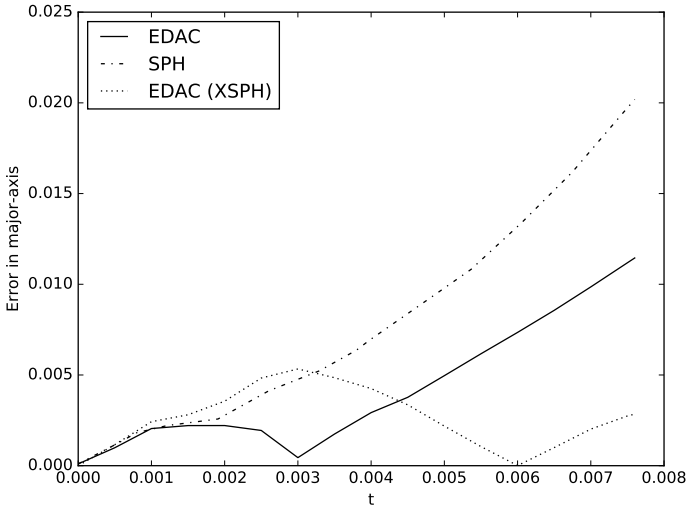

Figure 19: The error in the computed size of the semi-major axis compared for the standard SPH, EDAC and the EDAC with the use of XSPH.

the XSPH correction and Fig. 23 shows the particles and the pressure distribution using the EDAC scheme along with the XSPH correction. The XSPH correction seems to reduce the noise in the particle distribution. It is clear that the EDAC scheme has much lower pressure oscillations than the WCSPH scheme even though no artificial viscosity is used.

As can be seen, the new scheme outperforms the standard SPH scheme in general, conserves kinetic energy, has lower pressure oscillations, and is quite robust as there is no need for an artificial viscosity to keep the scheme stable.

4.7. Hydrostatic tank

The next example is a simple benchmark to ensure that the pressure is evolved correctly. This benchmark consists of a tank of water held at rest as simulated by Adami et al. [18]. The fluid is initialized with a zero pressure with the particles at rest. The acceleration due to gravity is set to -1m/s^2, the height of the water is 0.9m and the density of the fluid is set to 1000kg/m^3. The maximum speed of the fluid is taken to be $\sqrt{gH}$ and the speed of sound is set to ten times this value. The timestep is calculated as before using these values. The acceleration due to gravity is damped as discussed in

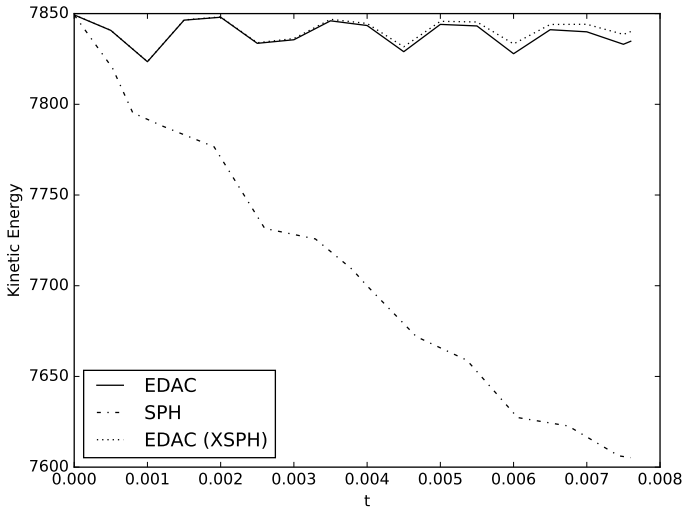

Figure 20: The kinetic energy of the elliptical drop computed by different schemes.

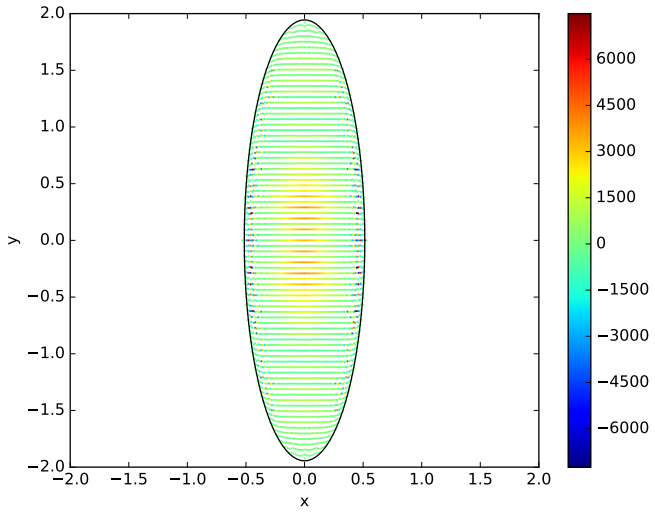

Figure 21: The distribution of particles for the elliptical drop problem at $t = 0.0076$ seconds using the standard WCSPH scheme with the use of artificial viscosity. The solid line is the exact solution and the colors indicated the pressure.

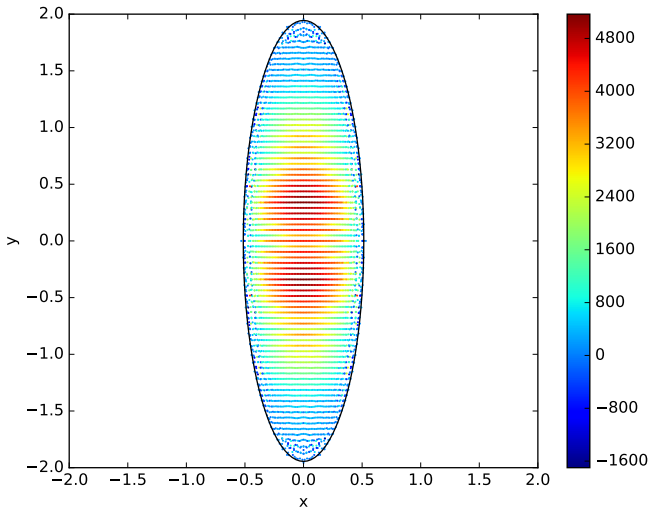

Figure 22: The distribution of particles for the elliptical drop problem at $t = 0.0076$ seconds using the EDAC scheme without the addition of the XSPH correction. No artificial viscosity is used in the simulation. The solid line is the exact solution and the colors indicated the pressure.

[18]. In order to reproduce the results, the same artificial viscosity factor $\alpha = 0.24$ is used. No physical viscosity is used. The parameter α for the EDAC equation is set to 0.5. The problem is simulated with the TVF scheme (using no background pressure) as well as the EDAC scheme. To compare the results, the pressure is evaluated along a line at the center of the tank.

In Fig. 24 the pressure at the bottom of the tank is plotted versus time for both the TVF scheme and the EDAC scheme. The EDAC scheme seems to produce a bit more oscillation in the pressure but the overall agreement is good.

In Fig. 25, the pressure variation with height for a line of points at the center of the tank is plotted for different schemes at the times $t = 0.5$ and $t = 2$. The agreement is very good. This shows that the EDAC scheme produces good pressure distributions.

4.8. Water impact in two-dimensions

The case of two rectangular blocks of water impacting is considered next. A detailed study of this problem has been performed by Marrone et al. [25] in which they use a fully Compressible, Riemann-Solver type SPH formulation

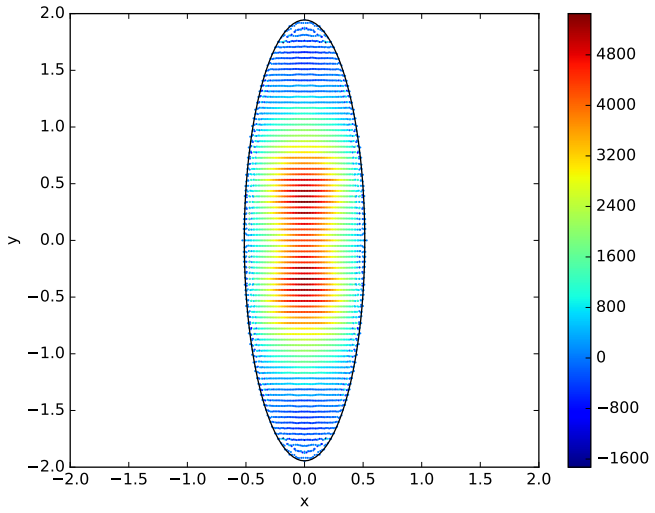

Figure 23: The distribution of particles for the elliptical drop problem at $t = 0.0076$ seconds using the EDAC scheme with the addition of the XSPH correction. No artificial viscosity is used in the simulation. The solid line is the exact solution and the colors indicated the pressure.

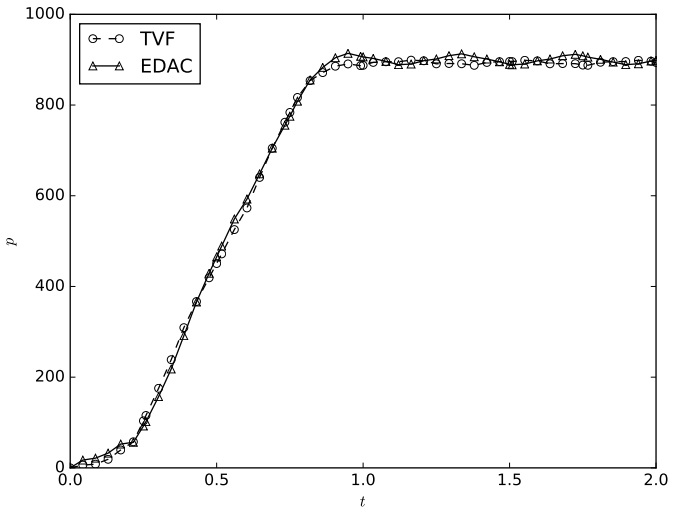

Figure 24: Plot of the pressure at the bottom of the tank versus time for different schemes.

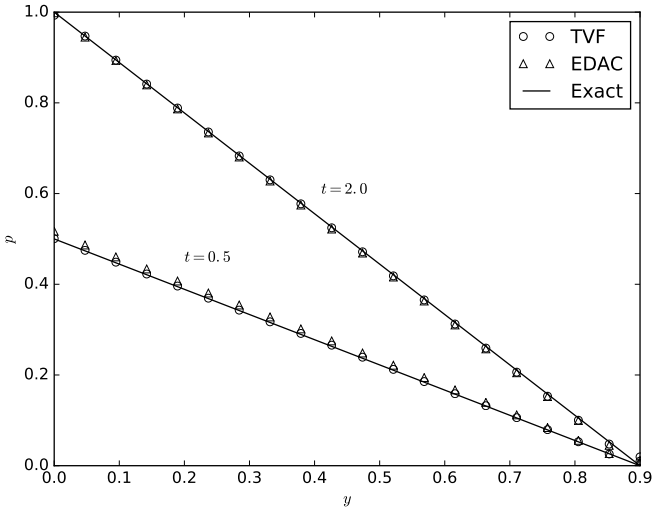

Figure 25: Pressure variation with height for the different schemes at $t = 0.5$ and $t = 2.0$.

and compare the results with a Least-Squares finite volume method. The problem involves two blocks of water, each with side H and height L, that are stacked vertically at $t = 0$, with the interface at $y = 0$. The top block moves down with the y-component of velocity $v = -U$ and the bottom moves up with velocity $v = U$. There is no acceleration due to gravity and the fluid is treated as inviscid and incompressible. Surface tension is not modeled. This is simulated using the standard EDAC scheme and also the WCSPH scheme. In the present case $L = 1m$, $H = 2m$, $U = 1m/s$ and $\rho = 1.0kg/m^3$. The Mach number is chosen to be 0.01. For the WCSPH scheme, $\gamma = 1$. A quintic spline kernel is used for both schemes with $h = \Delta x$ and $L/\Delta x = 100$. As considered in [25], the normalized pressure distribution $(p/\rho c_s U)$ is shown at $t^* = Ut/L = 0.007$ and at $t^* = Ut/L = 0.167$. When this case is run without any artificial viscosity, the traditional WCSPH scheme does not run successfully until the desired time. There are large pressure oscillations. Fig. 26 shows the particle distribution and pressure for the non-dimensionalized times of $t^* = 0.007$ (left) and $t^* = 0.1$ (right). In contrast, the EDAC case runs fairly well and the results are shown in Fig. 27. Initially, the pressure is comparable to the results in [25], however, the lack of any artificial viscosity results in small pressure oscillations at the final time and some cavitation. In Fig. 28 the same case is simulated with an artificial

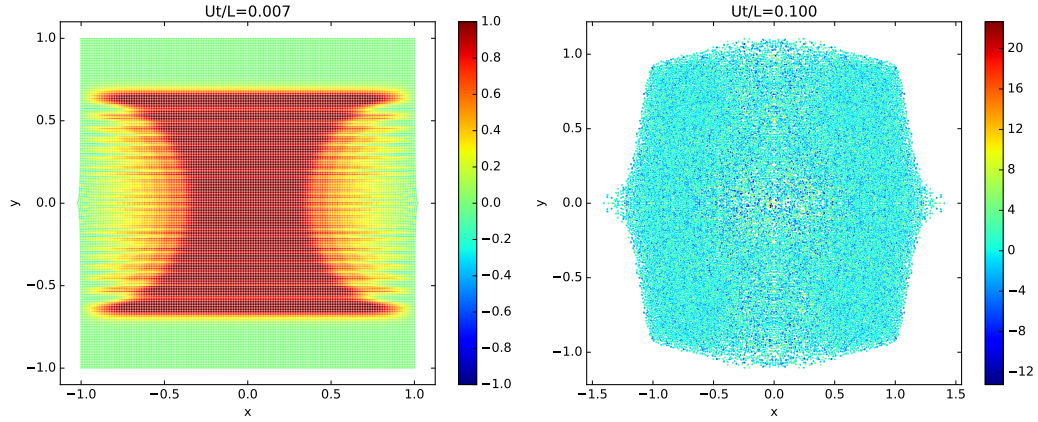

Figure 26: Particle distribution and pressure ($p/\rho c_s U$) at $Ut/L = 0.007$ (left) and $Ut/L = 0.1$ (right) for the water impact problem with the standard WCSPH scheme without any artificial viscosity.

viscosity with $\alpha = 0.1$. This produces fairly good results. It is easy to see that in all cases, the new scheme produces much less pressure oscillations. It is worth noting that while the WCSPH scheme requires the use of artificial viscosity for the simulation to complete, it displays high-frequency pressure oscillations as can be seen in Fig. 29, where the artificial viscosity parameter $\alpha = 0.1$ was used for the WCSPH scheme. These results clearly show the superiority of the new scheme.

4.9. Dam-break in two-dimensions

The two-dimensional dam break over a dry bed is considered next. This problem cannot be simulated by the TVF scheme. The results are instead compared with a standard SPH implementation. The suggested corrections of Hughes and Graham [26] and Marrone et al. [27] are also employed in the implementation of the standard SPH scheme as provided in PySPH. In the current work, only the corrections of Hughes and Graham [26] are used. The delta-SPH corrections of Marrone et al. [27] do not affect the present results.

The problem considered is as described in Gomez-Gesteria et al. [28] with a block of water $1m$ wide and $2m$ high, placed in a vessel of length $4m$. The block is released under the influence of gravity which is assumed to be $-9.81m/s^2$. To compare the results, the position of the toe of the dam versus time is plotted and compared with the experimental results extracted from Koshizuka and Oka [29]. The particles are arranged as per a staggered

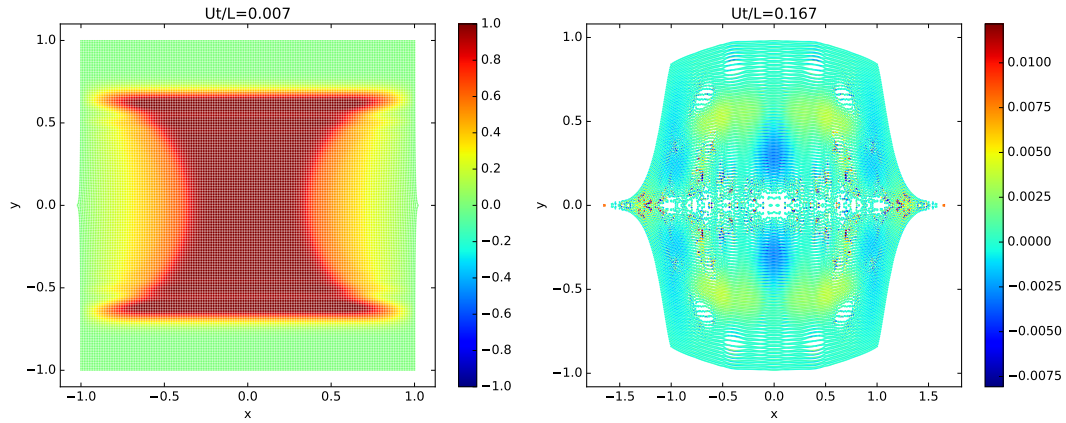

Figure 27: Particle distribution and pressure ($p/\rho c_s U$) at $Ut/L = 0.007$ (left) and $Ut/L = 0.167$ (right) for simulation with the standard EDAC scheme without any artificial viscosity.

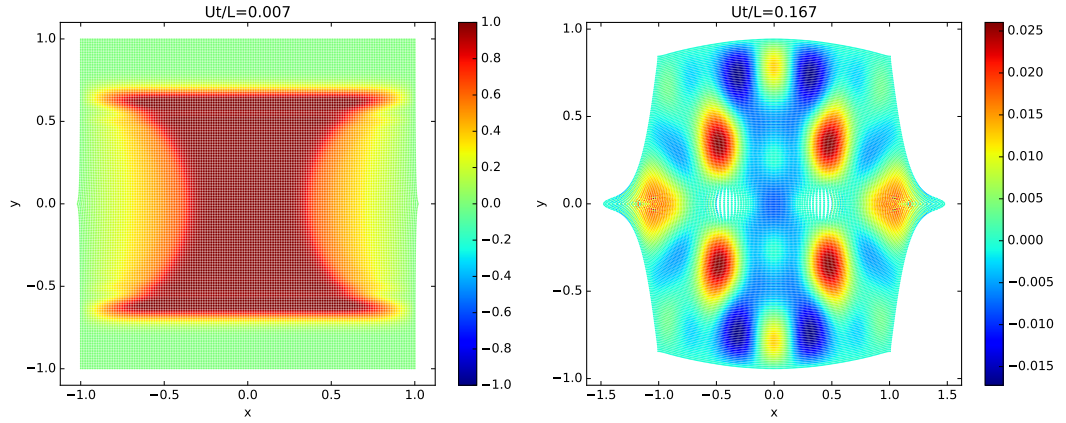

Figure 28: Particle distribution and pressure at $Ut/L = 0.007$ (left) and $Ut/L = 0.167$ (right) for simulation with the standard EDAC scheme with artificial viscosity coefficient $\alpha = 0.1$.

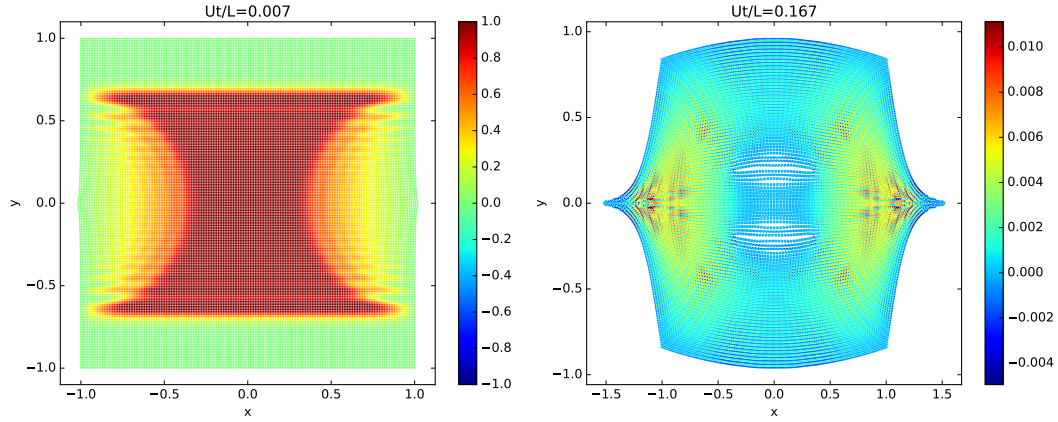

Figure 29: Particle distribution and pressure at $Ut/L = 0.007$ (left) and $Ut/L = 0.167$ (right) for simulation with the standard WCSPH scheme with artificial viscosity coefficient $\alpha = 0.1$.

grid as is suggested for the standard SPH formulation by Gomez-Gesteria et al. [28]. The highest resolution case uses $h = 0.0156$. Artificial viscosity is used for the WCSPH implementation with a value of $\alpha = 0.1, \beta = 0.0$. The standard Wendland quintic kernel is used for WCSPH case with $h = 1.3\Delta x$.

For the EDAC implementation, the same particle arrangement as for the WCSPH case is used. No artificial viscosity or XSPH correction is employed. A quintic spline kernel is used with $h = \Delta x$. The value of α for the is set to 0.5. The only change to the implementation is a clamping of the boundary pressure to non-negative values so as to prevent the fluid from sticking to the walls.

The results are plotted in Fig. 30. As can be seen, the results of the new scheme compare well with the experimental results and the WCSPH formulation. The figure also plots the results of the Moving Point Semi-implicit (MPS) scheme of [29]. The agreement is excellent. The difference between the computational results and those of the experiment are generally attributed to the fact that the simulations use an inviscid fluid.

4.10. Wave maker in two-dimensions

As a final case, a simplified wave-generator is considered. This case demonstrates the strength of the new scheme. The problem is a simplified version of the one simulated by Altomare et al. [30]. The problem consists of a vessel containing an incompressible fluid with the left wall of the vessel

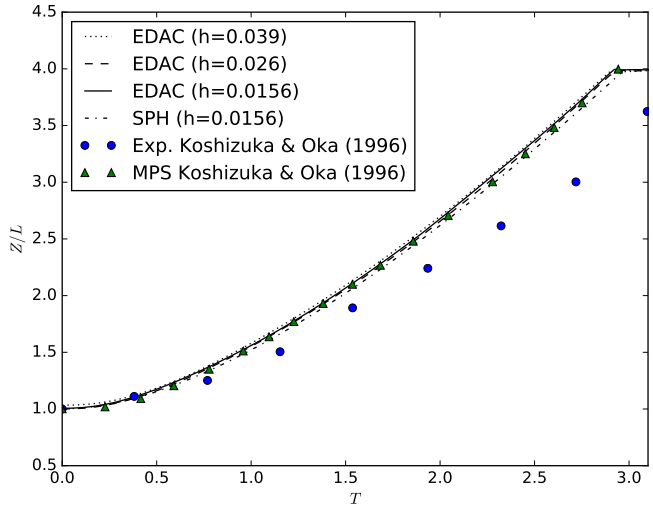

Figure 30: Position of the toe of the dam as a function of time compared with experimental results of [29]. The triangular symbols plot the results of the MPS simulation of [29]. Z is the distance of the toe of the dam from the left wall and L is the initial width of the dam.

moving periodically. The right and bottom walls are held fixed. The fluid column height is $0.27m$ and its initial width is $0.5m$. The forcing function for this is given as,

$$u(t) = \frac{H\omega(\sinh(kd)\cosh(kd) + kd)}{4\sinh^2(kd)}\cos(\omega t), \tag{26}$$

where $d = 0.27, k = 2\pi/1.89, H = 0.1$. At $t = 0$, the right side of the left wall is at $x = 0$.

This problem is simulated with the classic WCSPH scheme and with the new scheme. The simulation is run for a total time of 5 seconds. A timestep of 5×10^{-5} seconds is used. The density of the fluid is $1000kg/m^3$. Artificial viscosity is used and the value of $\alpha = 0.25$. The Predict-Evaluate-Correct (PEC) integrator is used for the EDAC scheme and an Evaluate-Predict-Evaluate-Correct (EPEC) integrator is used for the WCSPH scheme. The suggested corrections of Hughes and Graham [26] are used for the WCSPH scheme. The quintic spline kernel is used for all schemes with $\Delta x = 0.004$ and $h = \Delta x$. The fluid and boundary particles are initialized uniformly.

Fig. 31 shows the pressure along a vertical line at $x = 0.25$ at $t = 5s$.

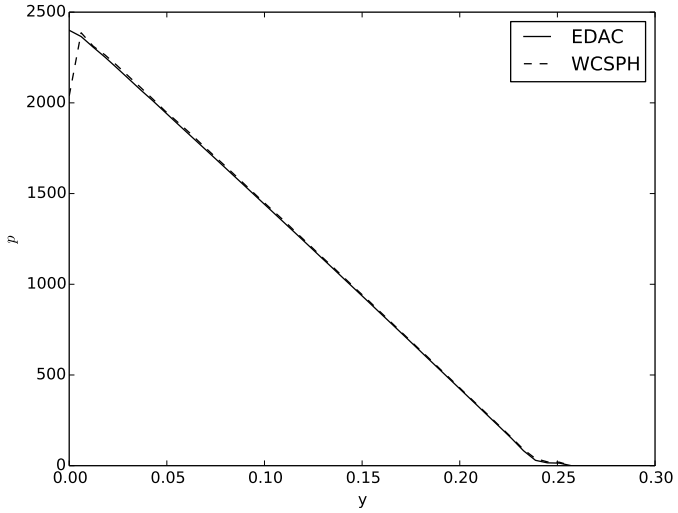

Figure 31: Plot of pressure interpolated on a line at $x = 0.25$ for the new scheme and with the classic WCSPH scheme at 5s.

As can be seen, the pressure for the new scheme is smooth even near the boundary at $y = 0$.

The minimum and maximum pressure in the fluid at $t = 5s$ is calculated and compared for the different schemes in Table 1. As can be seen, the EDAC scheme has the least pressure variation. In addition to the WCSPH and EDAC cases, the problem has also been simulated with the scheme of Adami et al. [18] and with the new scheme but without the use of any artificial viscosity. The new scheme works even without any artificial viscosity. However, the pressure distribution is more noisy while the maximum pressure is lower than the other schemes. None of the other schemes will work without an artificial viscosity and the particle positions will diverge within the first second of the simulation.

It is important to note that the particles diverge with the WCSPH scheme when the simulation is run beyond 11.85 seconds using the PEC integrator. This time increases if a more accurate integrator is used namely the EPEC integrator. However, the particles eventually diverge at 16.05 seconds in this case. The scheme of Adami et al. [18] also display a particle divergence at 14.8 seconds and exhibits some pressure oscillations although the magnitude of these oscillations are lower. The new scheme runs for 25 seconds and has

SPH Scheme	p_{min}	p_{max}
EDAC	-7.4	2799.9
EDAC w/o artificial viscosity	-782.4	3145.5
WCSPH	-78.9	5640.2
Adami, Hu, Adams[18]	-571.8	4395.4

Table 1: The minimum and maximum pressure for the different schemes at $t = 5s$.

much smaller pressure oscillations than the other schemes. The new scheme has not been run for longer times but it does not appear that the particle positions will diverge.

This clearly shows that the new scheme is extremely robust and produces excellent results.

5. Conclusions

In this work, the Entropically Damped Artificial Compressibility scheme of Clausen [9] is applied to SPH. Two flavors of the new scheme are developed, one which is suitable for internal flows where the Transport Velocity Formulation of Adami et al. [8] is employed along with the EDAC scheme. The key elements of the scheme are the use of the EDAC equation to evolve the pressure, the use of the transport velocity, and, importantly, a pressure correction as suggested by Basa et al. [19]. This scheme outperforms the TVF scheme for the Taylor Green vortex problem at a variety of Reynolds numbers. The scheme performs very well for a variety of other internal flow problems. The standard EDAC scheme is easy to apply to external flow problems and to free-surface flows. The method produces results that are better than the standard SPH. The pressure distribution is smoother and more accurate. It does not require the use of artificial viscosity and is relatively simple to implement. It is seen that a judicious choice of the viscosity for the pressure equation is important. A heuristic expression is suggested that appears to work well for all the simulated problems. A fully working implementation of the scheme and all the benchmarks in this paper are made available in order to encourage reproducible computational science.

Acknowledgments

The authors are grateful to the anonymous reviewers for their comments that have made this manuscript better.

References

References

1. Lucy, L.B.. A numerical approach to testing the fission hypothesis. *The Astronomical Journal* 1977;82(12):1013–1024.

2. Gingold, R.A., Monaghan, J.J.. Smoothed particle hydrodynamics: Theory and application to non-spherical stars. *Monthly Notices of the Royal Astronomical Society* 1977;181:375–389.

3. Monaghan, J.J.. Simulating free surface flows with SPH. *Journal of Computational Physics* 1994;110:399–406.

4. Shadloo, M.S., Oger, G., Touze, D.L.. Smoothed particle hydrodynamics method for fluid flows, toward industrial applications: Motivations, current state, and challenges. *Computers & Fluids* 2016;136:11–34.

5. Violeau, D., Rogers, B.D.. Smoothed particle hydrodynamics (SPH) for free-surface flows: past, present and future. *Journal of Hydraulic Research* 2016;54:1–26.

6. Cummins, S.J., Rudman, M.. An SPH projection method. *Journal of Computational Physics* 1999;152:584–607.

7. Hu, X., Adams, N.. An incompressible multi-phase SPH method. *Journal of Computational Physics* 2007;227(1):264–278. URL: `http://linkinghub.elsevier.com/retrieve/pii/S0021999107003300`. doi:`10.1016/j.jcp.2007.07.013`.

8. Adami, S., Hu, X., Adams, N.. A transport-velocity formulation for smoothed particle hydrodynamics. *Journal of Computational Physics* 2013;241:292–307. URL: `http://linkinghub.elsevier.com/retrieve/pii/S002199911300096X`. doi:`10.1016/j.jcp.2013.01.043`.

9. Clausen, J.R.. Entropically damped form of artificial compressibility for explicit simulation of incompressible flow. *Physical Review E* 2013;87(1):013309–1–013309–12. URL: http://link.aps.org/doi/10.1103/PhysRevE.87.013309. doi:10.1103/PhysRevE.87.013309.

10. Clausen, J.R.. Developing Highly Scalable Fluid Solvers for Enabling Multiphysics Simulation. Tech. Rep. March; Sandia National Laborotories; 2013. URL: http://prod.sandia.gov/techlib/access-control.cgi/2013/132608.pdf.

11. Ansumali, S., Karlin, I.V., Öttinger, H.C.. Thermodynamic theory of incompressible hydrodynamics. *Physical Review Letters* 2005;94(8):1–4.

12. Karlin, I.V., Tomboulides, A.G., Frouzakis, C.E., Ansumali, S.. Kinetically reduced local Navier-Stokes equations: An alternative approach to hydrodynamics. *Physical Review E* 2006;74(3):6–9.

13. Borok, S., Ansumali, S., Karlin, I.V.. Kinetically reduced local Navier-Stokes equations for simulation of incompressible viscous flows. *Physical Review E* 2007;76(6):1–9.

14. Ramachandran, P., Puri, K.. Entropically damped artificial compressibility for SPH. In: Liu, G.R., Das, R., eds. *Proceedings of the 6th International Conference on Computational Methods 5 conference*; vol. 2. Auckland, New Zealand; 2015:Paper ID 1210. URL: http://www.sci-en-tech.com/ICCM2015/PDFs/1210-3216-1-PB.pdf.

15. Ramachandran, P., Puri, K.. PySPH: a framework for parallel particle simulations. In: *Proceedings of the 3rd international conference on particle-based methods (Particles 2013)*. Stuttgart, Germany; 2013:.

16. Ramachandran, P.. PySPH: a reproducible and high-performance framework for smoothed particle hydrodynamics. In: Benthall, S., Rostrup, S., eds. *Proceedings of the 15th Python in Science Conference*. 2016:127 – 135.

17. Morris, J.P., Fox, P.J., Zhu, Y.. Modeling low reynolds number incompressible flows using sph. *Journal of Computational Physics* 1997;136(1):214–226. doi:http://dx.doi.org/10.1006/jcph.1997.5776.

18. Adami, S., Hu, X., Adams, N.. A generalized wall boundary condition for smoothed particle hydrodynamics. *Journal of Computational Physics* 2012;231(21):7057–7075. URL: http://linkinghub.elsevier.com/retrieve/pii/S002199911200229X. doi:10.1016/j.jcp.2012.05.005.

19. Basa, M., Quinlan, N.J., Lastiwka, M.. Robustness and accuracy of SPH formulations for viscous flow. *International Journal for Numerical Methods in Fluids* 2009;60:1127–1148.

20. Ramachandran, P., Puri, K., et al. PySPH: a python-based SPH framework. 2010–. URL: http://pypi.python.org/pypi/PySPH/.

21. Monaghan, J.J.. Sph without a tensile instability. *Journal of Computational Physics* 2000;159:290–311.

22. Ghia, U., Ghia, K.N., Shin, C.T.. High-Re solutions for incompressible flow using the Navier-Stokes equations and a multigrid method. *Journal of Computational Physics* 1982;48:387–411.

23. Ellero, M., Adams, N.. SPH simulations of flow around a periodic array of cylinders confined in a channel. *International Journal for Numerical Methods in Engineering* 2011;86:1027–1040.

24. Monaghan, J.J.. On the problem of penetration in particle methods. *Journal of Computational Physics* 1989;82:1–15.

25. Marrone, S., Colagrossi, A., Di Mascio, A., Le Touzé, D.. Prediction of energy losses in water impacts using incompressible and weakly compressible models. *Journal of Fluids and Structures* 2015;54:802–822. doi:10.1016/j.jfluidstructs.2015.01.014.

26. Hughes, J., Graham, D.. Comparison of incompressible and weakly-compressible SPH models for free-surface water flows. *Journal of Hydraulic Research* 2010;48:105–117.

27. Marrone, S., Antuono, M., Colagrossi, A., Colicchio, G., Le Touzé, D., Graziani, G.. δ-SPH model for simulating violent impact flows. *Computer Methods in Applied Mechanics and Engineering* 2011;200:1526–1542. doi:10.1016/j.cma.2010.12.016.

28. Gomez-Gesteria, M., Rogers, B.D., Dalrymple, R.A., Crespo, A.J.. State-of-the-art classical SPH for free-surface flows. *Journal of Hydraulic Research* 2010;84:6–27.

29. Koshizuka, S., Oka, Y.. Moving-particle semi-implicit method for fragmentation of incompressible fluid. *Nuclear Science and Engineering* 1996;123:421–434.

30. Altomare, C., Suzuki, T., Domínguez, J.M., Barreiro, A., Crespo, A., Gómez-Gesteira, M.. Numerical wave dynamics using lagrangian approach: wave generation and passive and active wave absorption. 10th International SPHERIC workshop; Parma, Italy; 2015:.